



Deposited via The University of Leeds.

White Rose Research Online URL for this paper:

<https://eprints.whiterose.ac.uk/id/eprint/723/>

Article:

Collantes, J.M., Pollard, R.D. and Sayed, M. (2002) Effects of DUT mismatch on the noise figure characterization: A comparative analysis of two Y-factor techniques. IEEE Transactions on Instrumentation and Measurement, 51 (6). pp. 1150-1156. ISSN: 0018-9456

<https://doi.org/10.1109/TIM.2002.808015>

Reuse

See Attached

Takedown

If you consider content in White Rose Research Online to be in breach of UK law, please notify us by emailing eprints@whiterose.ac.uk including the URL of the record and the reason for the withdrawal request.

Effects of DUT Mismatch on the Noise Figure Characterization: A Comparative Analysis of Two Y-Factor Techniques

Juan-Mari Collantes, *Member, IEEE*, Roger D. Pollard, *Fellow, IEEE*, and Mohamed Sayed, *Member, IEEE*

Abstract—Device mismatch seriously degrades accuracy in noise figure characterization. The suitability of corrections to the gain definitions for a more precise noise figure evaluation for mismatched devices is investigated and compared to classical techniques. The effects of device mismatch on the noise figure of the noise-meter receiver and its impact on the final accuracy are analyzed.

Index Terms—Microwave characterization, noise figure, noise measurements, noise temperature, vector corrections, Y-factor technique.

I. INTRODUCTION

WITH the increasing need for high-performance components for use in mobile communications, the accurate measurement of the noise figure becomes an essential task. A significant number of procedures, addressing the issue of accurate noise figure calculation of circuits and devices, have been proposed in the recent literature [1]–[4]. The most common method for measuring the noise figure is the classical Y-factor technique, in which only noise power measurements are required [5]. Classical Y-factor is an accurate procedure for noise figure characterization provided that all the components involved in the measurement [noise source, device under test (DUT) and noise receiver] are well matched. However, because of the use of scalar noise power measurements alone, it cannot correct for the errors related to any mismatch present in the measurement path. In most cases, the noise source and the receiver are relatively well matched, and their effect can be neglected. Increasingly, there are requirements for mismatched devices to be measured, especially discrete active components (FETs, BJTs, etc.) presenting highly mismatched characteristics. Therefore, DUT mismatch becomes a critical issue in the noise figure characterization.

Recently, a specific technique has been proposed in order to deal with mismatch effects in the noise figure evaluation [3]. This technique combines the classical Y-factor method

with scattering parameter measurements. From these additional vector measurements, some corrections are performed on the classical procedure, the most important being those related to an accurate gain definition. The DUT gain is required in order to de-embed the noise figure of the DUT from the noise figure of the complete measurement system. The classical Y-factor technique makes use of the DUT insertion gain, since it is obtained through scalar measurements alone. Instead, the use of the DUT available gain, which can be computed from the measured S -parameters, is proposed in [3]. In the following, we will refer to the use of the available gain for the noise figure calculation instead of insertion gain as the *corrected Y-factor technique*.

In this work, the suitability of using the available gain and its actual effect on the measurement accuracy are analyzed and compared with the classical Y-factor technique. All the consequences derived from measurement of a mismatched DUT are investigated in detail. In particular, special attention is paid to the impact of DUT mismatch on the noise figure of the noise-meter receiver since this is required for the computation of the DUT noise figure. As the noise figure of the noise-meter receiver can be a strong function of the source impedance connected to its input, we can expect significant variations in the receiver noise figure versus DUT output match. Here, the effects of neglecting the receiver noise figure dependence on source impedance are rigorously examined. Although there are other sources of error in any noise figure measurement (ENR uncertainty, instrument uncertainty, presence of spurious signals, etc.), these are beyond the scope of this work.

It is first necessary to provide some basic definitions concerning the noise figure and related quantities and the fundamentals of the Y-factor method. Its implementation through the classical and the modified techniques is described, and an uncertainty analysis, comparing both techniques, is performed as a function of DUT gain and match. Finally, some experimental data is presented which confirms the theoretical analysis.

II. RELEVANT NOISE FIGURE BASICS

A. Noise Figure Definition

The noise figure is defined as the ratio of the signal-to-noise ratio (SNR) at the input of a two-port network to the SNR observed at the output when the input noise N_i corresponds to the

Manuscript received September 27, 2000; revised September 30, 2002. This work was supported in part by the University of the Basque Country.

J.-M. Collantes is with the Electricity and Electronics Department, University of the Basque Country, Bilbao, Spain.

R. D. Pollard is with the School of Electronic and Electrical Engineering, The University of Leeds, Leeds, U.K.

M. Sayed is with Agilent Technologies, Santa Rosa, CA 95403 USA.

Digital Object Identifier 10.1109/TIM.2002.808015

available thermal noise power of a resistive termination at a reference temperature T_0 (a value of $T_0 = 290$ K was first suggested by Friis [6])

$$F = \frac{S_i/N_i}{S_o/N_o} \Big|_{T=T_0} \quad (1)$$

where

S_i and S_o signal power levels available at the input and the output of the two-port network;

N_i and N_o available noise power at the input and the output of the two-port network.

N_o can be expressed as

$$N_o = N_{add} + G_a N_i \quad (2)$$

where

N_{add} noise power added by the two-port network;

G_a its available gain, which is described by

$$G_a = \frac{1 - |\Gamma_s|^2}{|1 - S_{11}\Gamma_s|^2} |S_{21}|^2 \frac{1}{1 - |\Gamma_{out}|^2}. \quad (3)$$

Here, S_{ij} are the S parameters of the two-port network, Γ_s the reflection coefficient of the source connected at the input of the two-port network, and Γ_{out} the output reflection coefficient of the two-port network

$$\Gamma_{out} = S_{22} + \frac{S_{12}S_{21}\Gamma_s}{1 - S_{11}\Gamma_s}. \quad (4)$$

Equation (1) can be rewritten as

$$F = \frac{N_{add} + kT_0BG_a}{kT_0BG_a} \quad (5)$$

which is the definition of the noise figure at the standard reference temperature, $T_0 = 290$ K, given by IEEE Standard [7].

B. Noise Parameters

A significant characteristic of the noise figure is that it is a function of the source impedance from which the device is fed. This dependence makes the noise figure an incomplete noise description of the device. The full characterization of the noise figure for all possible source terminations requires a set of four independent parameters. There are a variety of parameter sets that can be used to represent this dependence. One of the most commonly used sets is given by [8]

$$F(\Gamma_s) = F_{\min} + 4 \frac{R_n}{Z_0} \frac{|\Gamma_s - \Gamma_{opt}|^2}{|1 + \Gamma_{opt}|^2(1 - |\Gamma_s|^2)} \quad (6)$$

where Γ_s is the source reflection coefficient, Z_0 is the reference impedance, and F_{\min} , R_n , $\text{real}(\Gamma_{opt})$, and $\text{imag}(\Gamma_{opt})$ are the four classical noise parameters.

It is important to notice that, as Γ_s tends to the edge of the Smith chart, the noise figure of any two-port network tends to infinity at a rate that is mainly determined by R_n . In the limit, for a totally reflective source ($|\Gamma_s| = 1$) the noise figure is infinite, which is a straightforward result from (6).

C. Measuring Noise Figure: The Y-factor Method

The most widely used procedure to measure the noise figure is the Y-factor method [5]. It requires measurement of the noise power at the output of the DUT for two different (hot and cold) temperatures of the noise source. The ratio of these two power noise levels, N_c and N_h , is called the Y-factor, which gives the name to the technique

$$Y = \frac{N_h}{N_c}. \quad (7)$$

From (5) the noise figure can be expressed as a function of the hot and cold noise source temperatures T_h , T_c , the Y-factor and the reference temperature $T_0 = 290$ K

$$F = \frac{\left(\frac{T_h}{T_0} - 1\right) - Y \left(\frac{T_c}{T_0} - 1\right)}{Y - 1}. \quad (8)$$

Equation (8) assumes that the reflection coefficient of the noise source (Γ_s) remains constant from hot to cold states. In practice, some amount of variation in Γ_s should be expected. Since the noise figure is a function of the source impedance (6), Γ_s variations will lead to some amount of error when (8) is used for the noise figure calculation. However, changes in Γ_s from hot to cold states are small for typical commercial noise sources operated below 18 GHz and will be neglected in the following analyses.

D. Second-Stage Correction

Equation (8) represents an ideal approach to the noise figure characterization of a generic DUT. However, in any real characterization setup, the measurement system also adds its own noise to the total output measured noise power. A typical configuration for noise figure measurement is depicted in Fig. 1(a) where the DUT is cascaded with a real receiver that also contributes to the total output noise.

The global noise figure (F_{sys}) of the cascaded system comprising a DUT followed by a real receiver can be calculated from the measured output noise powers N_h and N_c by using (8). Then, the noise figure of the DUT can be de-embedded by making use of the Friis formula for the cascade of two stages:

$$F_{DUT}(\Gamma_s) = F_{sys}(\Gamma_s) - \frac{F_{rec}(\Gamma_{out}) - 1}{G_a} \quad (9)$$

where

- Γ_s reflection coefficient of the noise source;
- Γ_{out} output reflection coefficient of the DUT (4);
- G_a DUT available gain (3);
- F_{rec} noise figure of the receiver.

It is important to notice that, from (9), the noise figure of the DUT depends on three terms:

- the measured global noise figure of the system made up of the cascade of DUT and receiver, $F_{sys}(\Gamma_s)$;
- the noise figure of the receiver *when the DUT is connected to its input*, $F_{rec}(\Gamma_{out})$, i.e., when the source impedance connected to its input is equal to Γ_{out} ;
- the available gain of the DUT, G_a .

Equation (9) is often referred to as the second-stage correction. Note that, if the DUT has an available gain G_a large enough

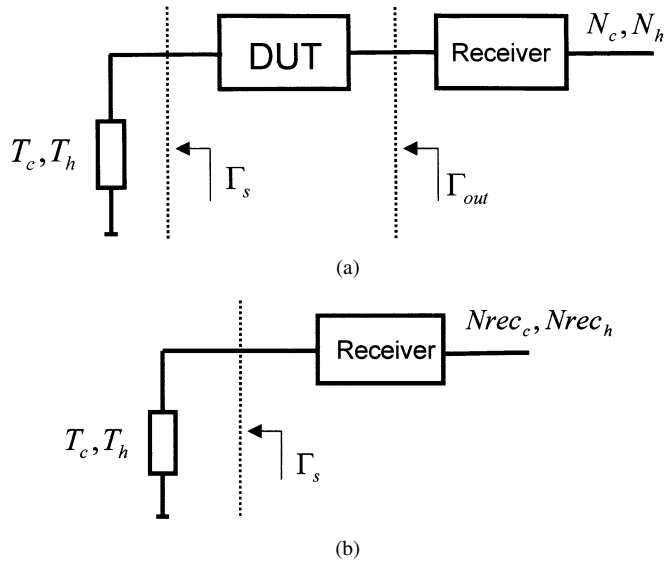


Fig. 1. Block diagram for noise figure measurements. (a) Measurement setup. The source impedance at the input of the receiver is Γ_{out} . (b) Calibration setup. The source impedance at the input of the receiver is Γ_s .

to make the second term of (9) negligible, then F_{DUT} becomes equal to F_{sys} . Otherwise, knowledge of all three terms is required to accurately determine the noise figure of the DUT.

III. TWO Y-FACTOR TECHNIQUES

Although (9) defines the “true” second-stage correction, it is almost invariably simplified in practice. Two noise-figure techniques that approximate (9) in two different ways are discussed next: the classical Y-factor technique and the corrected Y-factor technique. Both techniques are only approximations of the true second-stage correction. In both cases the quality of the approximation is a function of the DUT match and gain, and this is analyzed in the present work.

A. Classical Y-Factor Technique

This technique is the most extended way for measuring the noise figure, and it is based on noise power measurements exclusively [5]. The measurement procedure is divided into two steps. Step 1 is a calibration stage in which the noise source is directly connected to the receiver in order to measure the receiver noise figure. The calibration configuration is depicted in Fig. 1(b). The result is the value of the receiver noise figure for a source impedance Γ_s . Since the noise source has an attenuator pad at its output, it presents a reasonably good match and Γ_s is usually close to zero. Thus, in general, the result from the calibration step corresponds to the receiver noise figure for well-matched source impedance conditions, $F_{rec}(\Gamma_s)$. In step 2, the global noise figure F_{sys} of the cascaded system DUT and receiver is measured as shown in Fig. 1(a).

The available gain G_a of the DUT, that is also required in (9), cannot be determined from scalar power measurements alone. Therefore, this technique calculates the insertion gain G_{ins} instead. Insertion gain is usually measured as the ratio of the power delivered when the DUT is connected between the noise

source and the receiver to the delivered power when the noise source alone is directly connected to the receiver

$$G_{ins} = \frac{N_h - N_c}{N_{rec_h} - N_{rec_c}}. \quad (10)$$

The noise power measurements performed in steps 1 and 2 provide the data required to compute the insertion gain from (10). The insertion gain can also be expressed as

$$G_{ins} = \frac{|1 - S_{rec_{11}}\Gamma_s|^2}{|1 - S_{rec_{11}}\Gamma_{out}|^2} |S_{21}|^2 \frac{1}{|1 - S_{11}\Gamma_s|^2} \quad (11)$$

where:

- $S_{rec_{11}}$ S_{11} parameter (input reflection coefficient) of the receiver;
- S_{21} and S_{11} DUT S -parameters;
- Γ_s reflection coefficient of the noise source;
- Γ_{out} output reflection coefficient of the DUT (4).

Equation (11) is only equal to the available gain when the DUT is perfectly matched.

The classical Y-factor technique then computes the DUT noise figure from:

$$F_{DUT}(\Gamma_s) = F_{sys}(\Gamma_s) - \frac{F_{rec}(\Gamma_s) - 1}{G_{ins}}. \quad (12)$$

There are two potentially significant differences between the rigorous noise figure calculation from the true second-stage correction (9) and (12) used by the classical Y-factor technique:

- $F_{rec}(\Gamma_{out})$ is approximated by $F_{rec}(\Gamma_s)$;
- G_a is approximated by G_{ins} .

In the case of a highly mismatched DUT, the output reflection coefficient Γ_{out} (4) will differ greatly from Γ_s , and significant discrepancies between $F_{rec}(\Gamma_s)$ and $F_{rec}(\Gamma_{out})$ have to be expected. Only when the DUT is well-matched (mainly output match) does the receiver noise figure calculated during the calibration step [Fig. 1(b)] $F_{rec}(\Gamma_s)$ coincide with the receiver noise figure during the measurement step [Fig. 1(a)] $F_{rec}(\Gamma_{out})$.

Similarly, when the receiver and the noise source are perfectly matched, G_{ins} is equal to $|S_{21}|^2$. If, in addition, the DUT presents a good match, G_a also converges to $|S_{21}|^2$. Otherwise, G_{ins} can be significantly different from G_a , especially for DUTs presenting a high output mismatch.

B. Corrected Y-Factor

Some corrections for improving noise figure accuracy have been recently proposed in [3]. The most significant of them takes into account the DUT mismatch by using the available gain G_a in the second-stage correction, as required by (9). The available gain is calculated from the measured scattering parameters of the DUT. $F_{rec}(\Gamma_s)$ and $F_{sys}(\Gamma_s)$ are obtained through the same calibration and measurement steps as the classical technique [Fig. 1(a) and (b)]. As a result, the DUT noise figure is determined from:

$$F_{DUT}(\Gamma_s) = F_{sys}(\Gamma_s) - \frac{F_{rec}(\Gamma_s) - 1}{G_a}. \quad (13)$$

In this paper, we call (13) the corrected Y-factor technique. There is only one difference between the true second-stage correction (9) and (13):

- $F_{rec}(\Gamma_{out})$ is approximated by $F_{rec}(\Gamma_s)$.

The same discussion concerning the discrepancies between $F_{rec}(\Gamma_{out})$ and $F_{rec}(\Gamma_s)$ for mismatched DUTs that affected the classical Y-factor technique still holds for the corrected technique.

IV. UNCERTAINTY ANALYSIS

Equations (12) and (13) represent two different approximations of the true second-stage correction given by (9). Both approaches substitute the term $F_{rec}(\Gamma_{out})$ in (9) by the term $F_{rec}(\Gamma_s)$ measured during the calibration step. In addition, the classical technique also substitutes the available gain G_a by the measured insertion gain G_{ins} , while the corrected technique makes use of the correct available gain G_a obtained from measured S -parameters. In this section, the uncertainty in the noise figure calculation from the two approximations is analyzed.

Let $F_{classical}$ and $F_{corrected}$ be the noise figures calculated from the classical (12) and the corrected technique (13), respectively, and let F be the actual noise figure computed from the true second-stage correction of (9). We can define the errors (in dB) in the noise figure calculation derived from both techniques as

$$\Delta F_{classical} = 10 \log F_{classical} - 10 \log F \quad (14)$$

$$\Delta F_{corrected} = 10 \log F_{corrected} - 10 \log F. \quad (15)$$

From (9), (12), and (13), $\Delta F_{classical}$ and $\Delta F_{corrected}$ can be expressed as

$$\Delta F_{classical} = 10 \log \left(F + \frac{F_{rec}(\Gamma_{out}) - 1}{G_a} - \frac{F_{rec}(\Gamma_s) - 1}{G_{ins}} \right) - 10 \log(F) \quad (16)$$

$$\Delta F_{corrected} = 10 \log \left(F + \frac{F_{rec}(\Gamma_{out}) - F_{rec}(\Gamma_s)}{G_a} \right) - 10 \log(F). \quad (17)$$

$\Delta F_{classical}$ and $\Delta F_{corrected}$ can be computed analytically by knowing the DUT characteristics (noise figure F and S -parameters), the receiver characteristics (S_{rec11} and the four noise parameters), and the noise source reflection coefficient (Γ_s). It is important to recall that the errors given by eqs. (16) and (17) are exclusively related with the way the “true” second-stage correction is approximated by eqs. (12) and (13). Other uncertainty sources present in any type of noise figure measurement (ENR uncertainty, instrument uncertainty, etc.) are not included.

While the receiver and the noise source characteristics are fixed and unchanged for a given measurement system, DUTs of very different gain, match and noise figure may be measured. The example analysis evaluates $\Delta F_{classical}$ and $\Delta F_{corrected}$ as functions of the DUT gain and match using the parameters listed in Table I.

Some considerations concerning this analysis have to be highlighted.

- Equations (16) and (17) are not explicit functions of frequency. Therefore, frequency is not directly involved in the analysis. All the terms used to compute $\Delta F_{classical}$

TABLE I
VALUES OF PARAMETERS USED IN THE ANALYSIS

Receiver S_{11} (S_{rec11})	-20 dB \angle 110°
Receiver F_{min}	6 dB
Receiver Γ_{opt}	-20 dB \angle 70°
Receiver R_n	40 Ω
Noise source reflection coefficient (Γ_s)	-26 dB \angle -20°
DUT S_{11}	-10 dB \angle 45°
DUT S_{12}	-30 dB \angle -30°
DUT S_{21}	5, 10, 20 dB \angle -60°
DUT S_{22}	from -30 dB to -1 dB \angle -110°
DUT Noise Figure F	2 dB

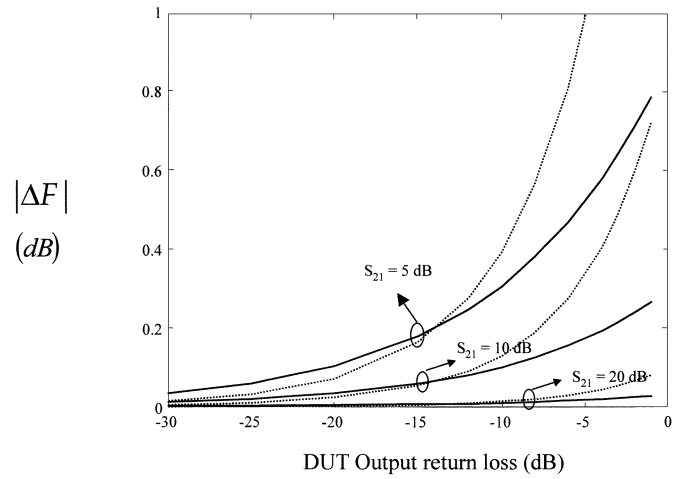


Fig. 2. Magnitude of the error versus DUT output return loss. Three values of S_{21} are considered. Characteristics of DUT, noise source and noise-meter receiver are listed in Table I. Solid line: classical. Dashed line: corrected.

and $\Delta F_{corrected}$ (receiver noise parameters, DUT S -parameters, DUT noise figure, etc.) are given at a single frequency point.

- The generic noise source and receiver, with common parameter values, are used in the analysis. Γ_s is a value typical of commercial noise sources used for applications below 18 GHz. The changes in Γ_s from hot to cold states are neglected.
- A DUT with noise figure $F = 2$ dB is used. The DUT output return losses will range from -30 dB to -1 dB. Input match is constant since the impact on the final error is less significant provided that the noise source is well matched. Three values of S_{21} are considered: 5, 10 and 20 dB.

V. RESULTS AND DISCUSSION

Fig. 2 shows the absolute value of the error in the noise figure obtained from the two techniques, versus the DUT output return losses, and for the different values of DUT S_{21} . Several general observations may be made.

- The errors provided by the two techniques decrease with device gain. This result is consistent with the fact that S_{21} is in the denominator of the second term of (9), (12), and

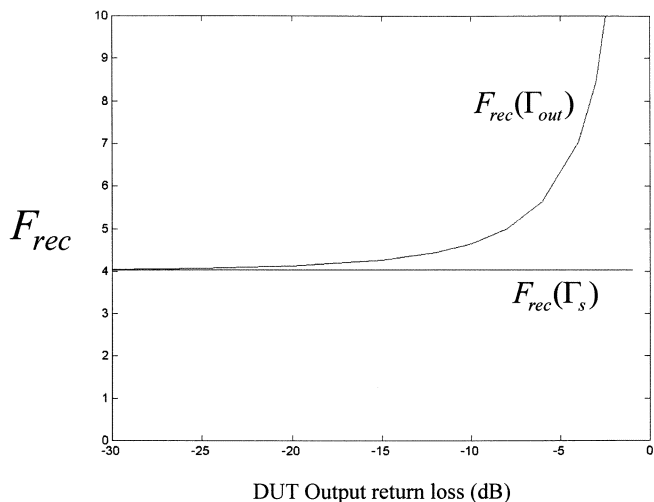


Fig. 3. Receiver noise figure F_{rec} as a function of DUT output return loss.

(13). High values of S_{21} make this second term negligible, and all three equations yield similar results.

- Errors are reduced in both techniques as the output return losses of the DUT decrease. This is due to the fact that, as the DUT output match improves, $F_{rec}(\Gamma_{out})$ converges to $F_{rec}(\Gamma_s)$, and G_a to G_{ins} (provided that the noise source and the receiver are reasonably well-matched, which is commonly the case).
- For low gain and high output mismatch both techniques provide a considerable amount of error.

The remarkable conclusion of this analysis is that, the corrected technique only presents a benefit for low values of the DUT output return loss, while the classical technique still provides a lower amount of error for high output return losses. This result may seem paradoxical given that the corrected technique makes use of the available gain G_a in order to better take into account mismatch effects, while the classical technique substitutes G_a by the insertion gain G_{ins} instead.

However, this phenomenon has a subtle explanation. The receiver noise figure F_{rec} and the DUT available gain G_a appearing in (9) are strong functions of the device output match through Γ_{out} [see (3) and (6)]:

- $F_{rec}(\Gamma_{out})$, in the numerator of (9), is inversely proportional to the term $1 - |\Gamma_{out}|^2$.
- $G_a(\Gamma_{out})$, in the denominator of (9), is also inversely proportional to the term $1 - |\Gamma_{out}|^2$.

In both cases, the term $1 - |\Gamma_{out}|^2$ becomes dominant as the DUT output match worsens ($|\Gamma_{out}| \rightarrow 1$), which makes G_a and F_{rec} tend to infinity. This is graphically shown in Figs. 3 and 4, where $F_{rec}(\Gamma_{out})$ and $G_a(\Gamma_{out})$ are plotted as functions of the DUT output return losses. The two curves are calculated considering the same receiver and noise source characteristics (Table I) and a DUT S_{21} of 5 dB. Superimposed in Fig. 3 is the receiver noise figure obtained from the calibration step $F_{rec}(\Gamma_s)$, which is obviously independent of Γ_{out} . Also, the insertion gain G_{ins} for the same DUT is plotted in Fig. 4, showing only a slight dependence on Γ_{out} . Since $F_{rec}(\Gamma_{out})$ and $G_a(\Gamma_{out})$ have the same form, they tend to compensate each other in (9). The corrected Y-factor combines $G_a(\Gamma_{out})$ —a

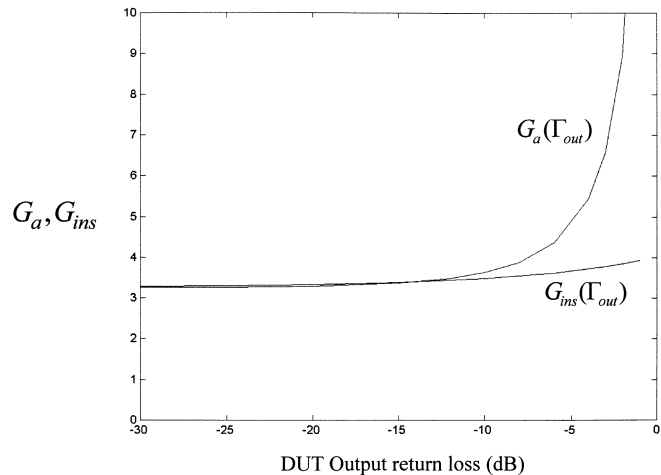


Fig. 4. Available gain G_a and insertion gain G_{ins} as functions of DUT output return loss.

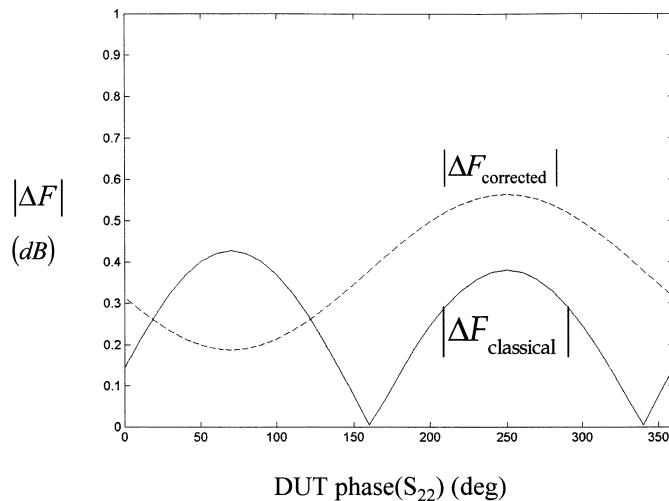


Fig. 5. Noise figure errors $|\Delta F_{classical}|$ and $|\Delta F_{corrected}|$ as functions of the DUT phase (S_{22}) for DUT characteristics: $S_{21} = 5$ dB, $S_{22} = -8$ dB, and $F = 2$ dB. (Other parameters as in Table I).

strong function of Γ_{out} —with $F_{rec}(\Gamma_s)$ —independent of Γ_{out} —resulting in large errors as the mismatch degrades. Conversely, the classical Y-factor combines $F_{rec}(\Gamma_s)$ with $G_{ins}(\Gamma_{out})$ that is only a mild function of Γ_{out} , which can result in a smaller total error.

This explanation is not necessarily a general result. Which one of the two techniques provides the more accurate results depends strongly on the receiver and DUT characteristics (receiver noise parameters, receiver match, DUT S -parameters, etc.). As a first example, Fig. 5 shows $|\Delta F_{classical}|$ and $|\Delta F_{corrected}|$ as a function of the phase of the DUT S_{22} . Other characteristics of the DUT are $S_{21} = 5$ dB, $S_{22} = -8$ dB and $F = 2$ dB with the remainder of the parameters involved in the analysis from Table I. Notice that errors strongly depend on phase conditions. Moreover, for some phases the smallest error is provided by the classical Y-factor technique, while for other phases the smallest error is associated with the corrected Y-factor.

As a second example, Fig. 6 shows the error associated with both techniques versus the receiver R_n parameter, for a specific DUT [$S_{21} = 5$ dB, $S_{22} = -5$ dB, $F = 2$ dB, phase ($S_{22}) =$

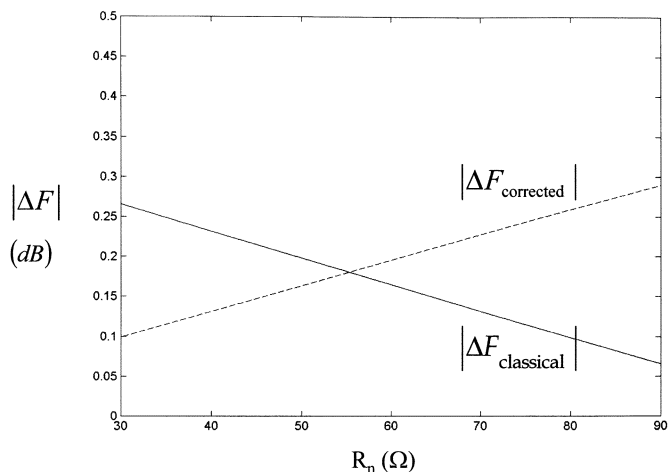


Fig. 6. Noise figure errors $|\Delta F_{classical}|$ and $|\Delta F_{corrected}|$ as functions of the receiver noise resistance R_n for DUT characteristics: $S_{21} = 5$ dB, $S_{22} = -5$ dB, phase (S_{22}) = 25° , and $F = 2$ dB. (Other parameters as in Table I).

25°]. The rest of the elements in the analysis are those from Table I. We can observe how, for this particular example, the classical Y-factor presents a smaller error for high R_n , whereas the corrected Y-factor is more accurate for low R_n .

Similar curves to Figs. 5 and 6 can be obtained by sweeping the other parameters involved in the analysis (F_{min} , Γ_{opt} ...), always resulting in the same conclusion: no general statement, valid for any arbitrary DUT and receiver characteristics, can be made about the suitability of using one of the two techniques, either or both of which may give highly erroneous results.

A precise application of the Y-factor method, suitable for low-gain, highly mismatched devices, would also need the evaluation of the term $F_{rec}(\Gamma_{out})$ in the second-stage correction (9). To do so, the four noise parameters of the receiver must be known or determined at a previous stage, so that $F_{rec}(\Gamma_{out})$ can be computed from (6).

VI. EXPERIMENTAL DATA

The results presented in the previous analysis have been verified with experimental data. The two Y-factor techniques have been applied to the noise figure measurement of five passive devices, each one having a different output match. These devices are built up combining a pad with different output mismatch blocks. Note that passive devices are selected for this experiment since their “true” noise figure can be calculated analytically from the S -parameters (for passive devices the noise figure is the inverse of the available gain). As a first step, the S -parameters of each device are measured at 1 GHz with a vector network analyzer. The resulting available gain and noise figure, computed from the S -parameters, are listed in Table II.

Then, the noise figures of the five devices were measured at 1 GHz through both the classical and corrected Y-factor techniques using a specific in-house noise-meter receiver with a noise figure of 4.1 dB and the HP 346B noise source. Note that the available gain calculated from the S -parameters (Table II) was used in the computation of the corrected Y-factor.

The errors associated with each technique ($\Delta F_{classical}$ and $\Delta F_{corrected}$) can be easily obtained since the “true” noise

TABLE II
DATA FOR EXPERIMENTAL DEVICES COMPUTED FROM THE MEASURED S -PARAMETERS AT 1 GHz

Test Device	S_{22}	G_{av}	F
1	-40 dB	-2.7 dB	2.7 dB
2	-16.8 dB	-3.0 dB	3.0 dB
3	-8.9 dB	-4.7 dB	4.7 dB
4	-4.5 dB	-2.3 dB	2.3 dB
5	-2.8 dB	-2.4 dB	2.4 dB

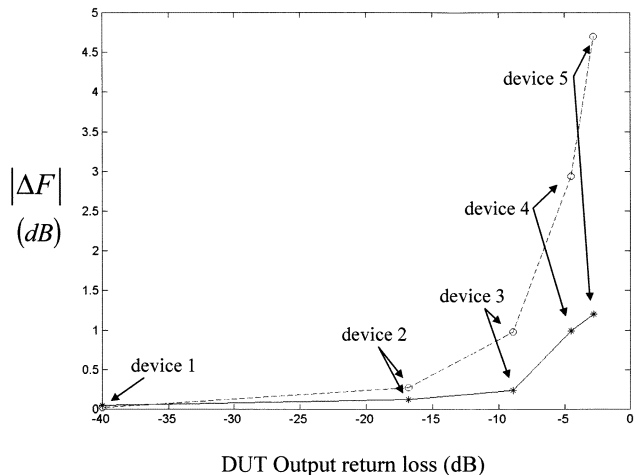


Fig. 7. Measured $|\Delta F_{classical}|$ and $|\Delta F_{corrected}|$ for five devices with different output return loss. Solid line: classical. Dashed line: corrected.

figures of the five passive devices have already been determined from the measured S -parameters. Fig. 7 shows $|\Delta F_{classical}|$ and $|\Delta F_{corrected}|$ as a function of the device output return loss. As expected, both errors dramatically increase as the device output match worsens. It is important to note that, since the gain of these passive devices is lower than unity, the mismatch errors are significantly higher. Nevertheless, for this series of experiments, results were always better with the classical Y-factor technique, confirming that there is no general benefit gained by using the available gain to correct the results when the DUT output return loss is high. In addition, the experiments yielded similar outcomes regardless of any additional cable length (phase shift) added to the devices.

VII. CONCLUSION

The impact of DUT mismatch effects on the accuracy in noise figure evaluation has been investigated for two different Y-factor-based techniques: the classical Y-factor technique, where only noise power measurements are involved, and the corrected Y-factor technique, in which DUT S -parameters are also measured in order to compute the DUT available gain. It has been shown that significant errors are provided by the two techniques when analyzing low-gain mismatched devices. These errors are mainly related to the neglect of the DUT mismatch effect on the noise figure of the noise-meter receiver. Moreover, results showed that, in general, the use of the available gain instead of insertion gain does not necessarily

ensure a more accurate result for high values of DUT output return losses. Errors from both techniques are strong functions of the receiver and DUT characteristics.

ACKNOWLEDGMENT

The authors would like to thank B. Shoulders of Agilent Technologies for helpful discussions.

REFERENCES

- [1] C. E. Collins, R. D. Pollard, R. E. Miles, and R. G. Dildine, "On the measurement of SSB noise figure using sideband cancellation," *IEEE Trans. Instrum. Meas.*, vol. 45, pp. 721–727, June 1996.
- [2] R. Drury, R. D. Pollard, and C. M. Snowden, "W-band noise figure measurement designed for on-wafer characterization," in *IEEE MTT-S Int. Microwave Symp. Dig.*, 1996, pp. 1273–1276.
- [3] D. Vondran, "Noise figure measurement: Corrections related to match and gain," *Microwave J.*, pp. 22–38, Mar. 1999.
- [4] S. C. Bundy, "Noise figure, antenna temperature and sensitivity level for wireless communications receivers," *Microwave Journal*, pp. 108–116, Mar. 1998.
- [5] "Fundamentals of RF and microwave noise figure measurements," Hewlett-Packard Application Note 57-1, Palo Alto, CA, July 1983.
- [6] H. T. Friis, "Noise figures of radio receivers," *Proc. IRE*, pp. 419–422, July 1944.
- [7] "Description of the noise performance of amplifiers and receiving systems," *Proc. IEEE*, pp. 436–442, Mar. 1963. Sponsored by IRE subcommittee 7.9 on Noise.
- [8] G. Gonzalez, *Microwave Transistor Amplifiers*. Englewood Cliffs, NJ: Prentice-Hall, 1984.

Juan-Mari Collantes (M'96) was born in Bilbao, Spain, in 1966. He received the degree in electronic physics from the University of the Basque Country, Spain, in June 1990 and the Ph.D. degree in electronics from the University of Limoges, Limoges, France, in March 1996. In December 1997, he received the Ph.D. degree in electronics from the University of Cantabria, Cantabria, Spain.

Since February 1996, he has been an Associate Professor in the Electricity and Electronics Department, University of the Basque Country. From July to December 1996, he was a Visiting Researcher at Hewlett-Packard, Santa Rosa, CA. His areas of interest include nonlinear analysis of microwave circuits, nonlinear modeling of microwave devices, and noise characterization at microwave frequencies.



Roger D. Pollard (M'77–SM'91–F'97) was born in London, U.K., in 1946. He received the B.Sc. and Ph.D. degrees in electrical and electronic engineering from the University of Leeds, Leeds, U.K.

He holds the Agilent Technologies Chair in High Frequency Measurements and is Head of the School of Electronic and Electrical Engineering, University of Leeds, where he has been a faculty member since 1974. He is an active member of the Institute of Microwaves and Photonics (one of the constituent parts of the School) which has over 40 active researchers,

a strong graduate program, and has made contributions to microwave passive and active device research. The activity has significant industrial collaboration as well as a presence in continuing education. Professor Pollard's personal research interests are in microwave network measurements, calibration and error correction, microwave and millimeter-wave circuits, terahertz technology, and large-signal and nonlinear characterization. He has been a consultant to Agilent Technologies (previously Hewlett-Packard Company), Santa Rosa, CA, since 1981. He has published over 100 technical articles and three patents.

Prof. Pollard is a Chartered Engineer and a Fellow of the Institution of Electrical Engineers (U.K.). He is an active IEEE volunteer (as an elected member of the Administrative Committee and 1998 President of the IEEE Microwave Theory and Techniques Society and as 2001/2002 Chair of the Products Committee) and a Member of the IEEE Technical Activities Board and Vice-Chair of the Publications, Services and Products Board (PSPB). He was Chair (1998 to 2000) of the TAB/PAB Electronic Products Committee which was responsible for the development and introduction of *IEEEExplore*. He has served as Chair of the UKRI Section and on many volunteer committees, groups, and working parties. He is a member of the Editorial Board of *IEEE TRANSACTIONS ON MICROWAVE THEORY AND TECHNIQUES* and has been on the Technical Program Committee for the IEEE Microwave Theory and Techniques International Microwave Symposium since 1986. He edits the IEEE Press book series on RF and microwave technology.

Mohamed Sayed (M'73) was born in Cairo, Egypt. He received the B.S. and M.S. degrees in electrical engineering from Cairo University, Cairo. He received the Ph.D. degree from Johns Hopkins University (JHU), Baltimore, MD.

He was with Hewlett-Packard for 27 years and with Agilent Technologies for three years. He is currently an Engineering Project Manager of microwave vector network analyzers. He taught graduate and undergraduate courses at Cairo University, JHU, Howard University, Washington, DC, and San Jose State University, San Jose, CA. He has authored and coauthored over 32 publications in the field of device characterization, microwave and millimeter-wave measurement systems, and high power amplifier design.

Dr. Sayed was the Technical Program Chairman of the 46th ARFTG held in San Francisco, June 1996, and Session Chairman at the 2000 European Microwave Conference held in Paris, France.